

What Causes the Pulse Power Saturation of GaAs-Based Broad-Area Lasers?

Joachim Piprek^{ID}, Senior Member, IEEE, and Zhan-Ming Li

Abstract—With short current pulses, the output power of semiconductor lasers is limited by non-thermal internal loss mechanisms. Two-photon absorption (TPA) was recently proposed as dominating photon loss process. We investigate this claim by advanced numerical laser simulation that includes all relevant mechanisms self-consistently. Using common material parameters, we obtain good agreement with the measured performance up to 90-W output power. Carrier leakage and free-carrier absorption are identified as the main saturation mechanisms, followed by longitudinal spatial hole burning. Contrary to earlier studies, TPA and gain compression are found negligible.

Index Terms—Semiconductor lasers, numerical analysis.

HIGH-POWER laser diodes [1], [2] are in demand for various applications, from solid state laser pumping to automotive light detection and ranging (LiDAR) [3]. In continuous-wave (CW) operation, the maximum power is usually limited by the self-heating of the laser [4]. Much higher power can be achieved in pulsed operation which largely eliminates self-heating effects [5]. Maximum pulse powers beyond 100W have been reported for broad-area lasers based on GaAs and emitting at wavelengths near 1000nm [6]. However, even with pulses as short as 10ns, saturation effects still limit the achievable power [7]. Based on different laser models, several mechanisms have been found responsible for the pulse power saturation. Wang et al. [8] used a two-dimensional electro-optic model and identified electron leakage from the active layers as root cause of the power saturation. Longitudinal spatial hole burning (LSHB) was also relevant. Free-carrier absorption (FCA) was very small and gain compression was declared negligible, despite a relatively large gain compression factor of $70 \times 10^{-17} \text{cm}^3$ in their model. Using a very similar model, Wenzel et al. [5] recognized a large influence of carrier recombination and FCA inside the waveguide layers as well as LSHB. They employed a large gain compression factor to reproduce the power vs. current (PI) measurement with their model. However, based on a one-dimensional traveling-wave optical model, Dogan et al. [9] explained the PI sub-linearity solely by two-photon absorption (TPA) and subsequent free-carrier absorption. This secondary FCA effect was caused by

Manuscript received February 21, 2018; revised March 27, 2018; accepted April 10, 2018. Date of publication April 13, 2018; date of current version April 27, 2018. (Corresponding author: Joachim Piprek.)

J. Piprek is with the NUSOD Institute LLC, Newark, DE 19714-7204 USA (e-mail: piprek@nusod.org).

Z.-M. Li is with Crosslight Software, Inc., Vancouver, BC V5M 2A4, Canada.

Color versions of one or more of the figures in this letter are available online at <http://ieeexplore.ieee.org>.

Digital Object Identifier 10.1109/LPT.2018.2826979

TABLE I
EPITAXIAL LASER STRUCTURE (GRIN –GRADED INDEX) [5]

Layer	Composition	Thickness	Doping
p-cladding	Al _{0.25} Ga _{0.75} As	25 nm	$2 \times 10^{18} \text{cm}^{-3}$
p-GRIN	GaAs - Al _{0.25} Ga _{0.75} As	1500 nm	0.1 - $2 \times 10^{18} \text{cm}^{-3}$
p-waveguide	GaAs	700 nm	$5 \times 10^{16} \text{cm}^{-3}$
p-waveguide	GaAs	100 nm	$1 \times 10^{16} \text{cm}^{-3}$
barrier	GaAs	10 nm	
quantum well	In _{0.29} Ga _{0.71} As	7nm	
barrier	GaAs	50 nm	
quantum well	In _{0.29} Ga _{0.71} As	7nm	
barrier	GaAs	50 nm	
quantum well	In _{0.29} Ga _{0.71} As	7nm	
barrier	GaAs	50 nm	
n-waveguide	GaAs	1300nm	$1 \times 10^{16} \text{cm}^{-3}$
n-waveguide	GaAs	300nm	$1 \times 10^{17} \text{cm}^{-3}$
n-waveguide	GaAs	200nm	$2 \times 10^{17} \text{cm}^{-3}$
n-waveguide	GaAs	100nm	$5 \times 10^{17} \text{cm}^{-3}$
n-cladding	Al _{0.25} Ga _{0.75} As	100 nm	$5 \times 10^{17} \text{cm}^{-3}$
n-cladding	Al _{0.25} Ga _{0.75} As	200 nm	$1 \times 10^{18} \text{cm}^{-3}$

TPA-generated carriers and it exceeds the primary TPA at high power. However, their model ignores carrier transport effects and employs the free-carrier lifetime of 2.7ns within the waveguide layers as fit parameter to find agreement with the same PI measurement used as reference by the other authors [5], [8].

In order to clarify these contradicting results, we here employ an improved two-dimensional electro-optic model that self-consistently includes all the saturation mechanisms mentioned above. This model was implemented in the PICS3D software [10] which was previously shown to deliver excellent agreement with measurements on similar lasers [11]. It solves the semiconductor drift-diffusion equations as well as the optical equations in vertical and longitudinal direction for a broad-area Fabry-Perot laser. TPA inside the waveguide layers is included as carrier generation process, so that TPA-generated carriers as well as injected carriers follow the same transport mechanisms and both contribute to FCA. More details on model and parameters are published elsewhere [12].

As example device we employ the same broad-area laser structure as above (Tab. 1) [5], [8], [9], so that the same

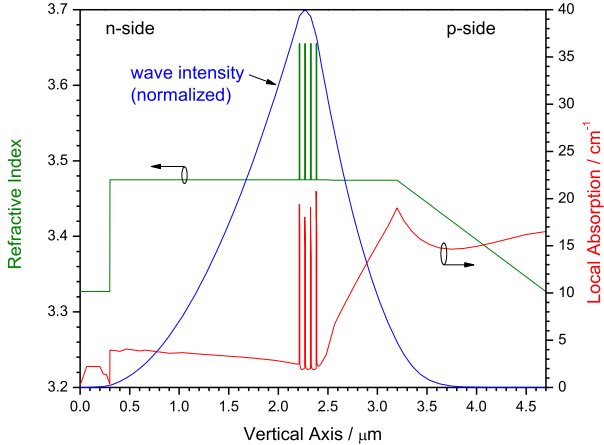


Fig. 1. Vertical profiles of refractive index, wave intensity (normalized), and local absorption at the front facet at 240A current.

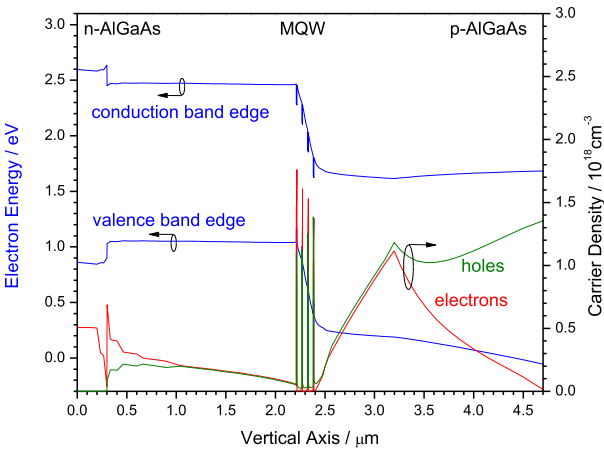


Fig. 2. Vertical profiles of energy band diagram and carrier density at the front facet at 240A current. MQW – multi-quantum well.

pulsed PI measurement can be used for model verification. The laser cavity length is $L = 4\text{mm}$ and the lasing stripe width is $W = 0.1\text{mm}$ with facet reflectivities of 0.01 at the front and 0.95 at the back. The laser structure includes an InGaAs/GaAs multi-quantum well (MQW) active region emitting at 1060nm as well as an AlGaAs graded-index (GRIN) layer.

The vertical index profile of the waveguide region and the optical intensity are plotted in Fig. 1. The guided laser mode is almost completely confined within the GaAs waveguide, so that an uniform TPA coefficient of $\beta = 26\text{cm/GW}$ can be employed as measured for GaAs at the same wavelength [13]. Our initial FCA cross-section is the same as in two previous studies [5], [9], $4 \times 10^{-18}\text{cm}^2$ for electrons and $12 \times 10^{-18}\text{cm}^2$ for holes. Wang et al used much lower FCA cross-sections [8]. FCA by holes is also referred to as intervalence-band absorption (IVBA). The local absorption profile at $I = 240\text{A}$ pump current is shown in Fig. 1 and it reveals strong IVBA within the p-side waveguide. Figure 2 plots the carrier density profiles together with the energy band diagram. Electrons leak out of the MQW into the p-side waveguide where they attract holes which mainly produce the strong absorption in Fig. 1. The graded bandgap of the p-AlGaAs GRIN layer leads to hole

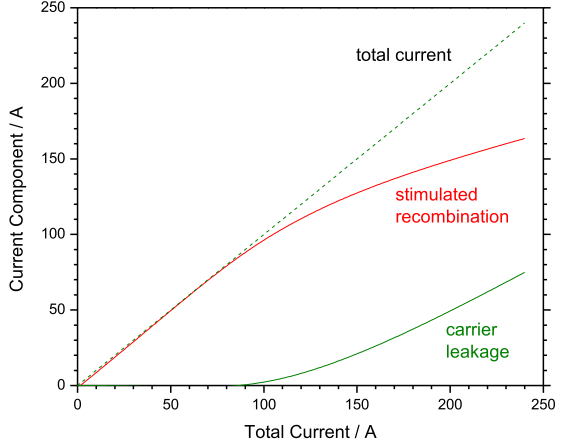


Fig. 3. Main current components vs. total current.

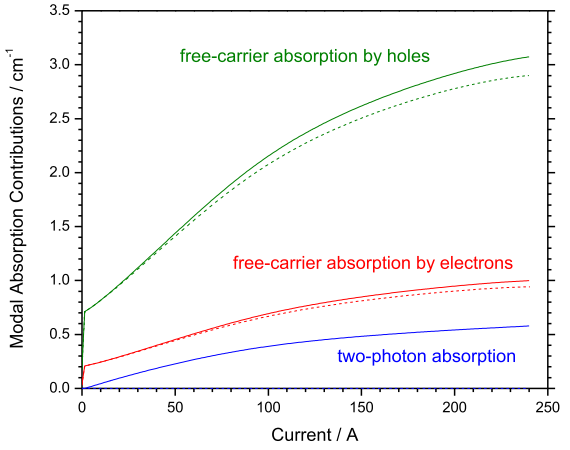


Fig. 4. Contributions of the different absorption mechanisms to the modal optical loss vs. current. Solid lines: full model. Dashed lines: no two-photon absorption.

accumulation in the tail region of the guided mode. The GRIN layer electron density drops strongly towards the p-cladding. However, most of the leaking electrons travel all the way to the p-contact at high current injection.

The total leakage current is plotted in Fig. 3 together with the current consumed by stimulated recombination within the QWs. At the maximum current of 240A, 68% of the injected carriers generate photons for the lasing mode while 31% are lost to leakage. The remaining 1% is consumed by carrier loss mechanisms inside the QWs. Thus, even without any absorption, carrier leakage causes significant power saturation above 100A. Electron leakage is much stronger than hole leakage. However, about 30% of the injected hole current is captured by leaked electrons at 240A so that these holes never reach the QWs.

Some of the leaked electrons accumulate in the p-waveguide and attract a similar number of holes which cause stronger FCA than electrons. Additional electron-hole pairs are generated by two-photon absorption and also cause FCA. Figure 4 compares the contributions from different absorption mechanisms. FCA by holes clearly dominates, including a small contribution from TPA-generated carriers. But

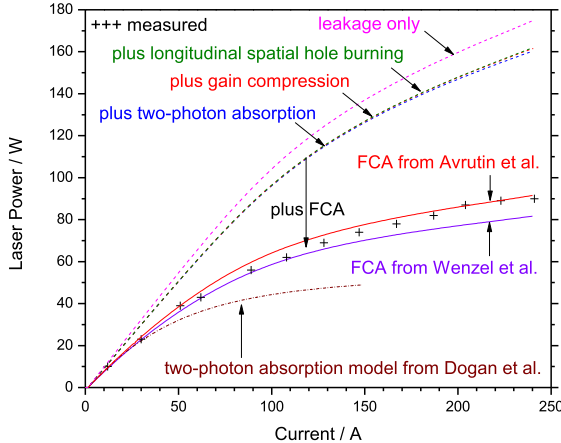


Fig. 5. Laser power vs. current as measured (+ + +) and as simulated with the full model (solid lines). The dashed lines show the simulation results after subsequent addition of key mechanisms to the model. FCA – free carrier absorption.

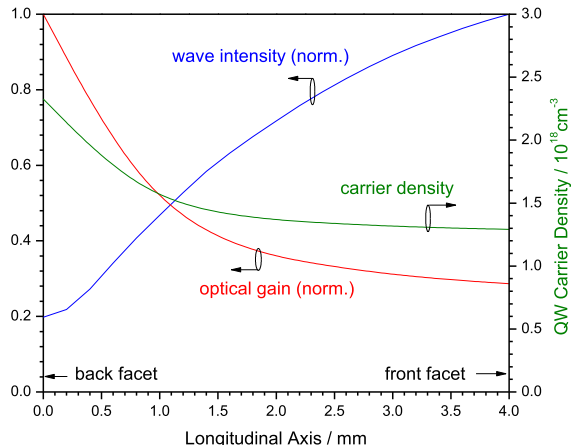


Fig. 6. Longitudinal profiles of optical intensity, QW gain, and average QW carrier density within the n-side QW.

the primary TPA is less important, as confirmed by other authors [14].

Figure 5 plots simulated PI characteristics in comparison to the measurement [5]. In order to quantify the different saturation mechanisms, we subsequently add them to the simulation in the following. The sub-linearity of the top curve is only produced by carrier leakage which is attributed to MQW conduction band edge deformations as illustrated in Fig. 2. In this case, we enforce a constant longitudinal distribution of carriers. By removing this restriction, we allow for longitudinal spatial hole burning (LSHB) which produces a somewhat lower power in Fig. 5. Longitudinal profiles of wave intensity, carrier density, and optical gain are shown in Fig. 6. The strongly asymmetric facet reflectivity produces the highest internal optical intensity at the front facet, so that stimulated recombination is strongest there and consumes more QW carriers than at the back facet. This LSHB effect leads to significant gain reductions near the front facet and to reduced output power.

The simulated power in Fig. 5 hardly changes after inclusion of gain compression using the common gain compression

factor of 10^{-17}cm^3 [2]. This phenomenological factor is often employed as fit parameter to find agreement with measurements so that other authors end up with much larger numbers compensating for power overestimations in their model [5], [7], [8].

Next, two-photon absorption is added to the model revealing a surprisingly small influence in Fig. 5 as discussed below. However, the final addition of free-carrier absorption causes the strongest power drop. Using our default FCA parameters from Wenzel et al. [5] leads to a lower power than measured at high current. The slightly smaller FCA cross-sections from Avrutin and Ryvkin [14] give a somewhat better agreement ($3 \times 10^{-18}\text{cm}^2$ for electrons and $10 \times 10^{-18}\text{cm}^2$ for holes). Published results of FCA measurements on GaAs vary and are rather uncertain at the low carrier densities present in our waveguide layers. However, this large FCA influence confirms earlier experimental investigations that observed a strong increase of the internal absorption with rising pulse current [15].

Despite our large TPA coefficient of $\beta = 26\text{cm/GW}$, we cannot confirm the strong TPA influence proposed by Dogan et al. for the same laser using a somewhat smaller $\beta = 15\text{cm/GW}$ [9]. Their TPA model leads to a significantly lower output power in our simulation (dash-dot line in Fig. 5) because it assumes that FCA by TPA-generated carriers rises with the third power of the local wave intensity. This assumption postulates that three photons are simultaneously involved, which is incorrect as TPA and FCA are separate processes.

Comparison of the calculated power at 240A allows for a ranking of saturation mechanisms. Both gain compression and TPA are irrelevant in our case as they only account for about 1W power loss each. LSHB is more important with 13W power drop, followed by FCA with 70W. A linear extrapolation of the top curve in Fig. 5 gives about 260W at 240A, so that carrier leakage produces a power drop of about 90W. In other words, electron leakage is the dominating high-power saturation mechanism in this laser.

At lower pulse power, leakage seems negligible in Fig. 3. However, even small leakage is accompanied by substantial carrier accumulation and FCA in the waveguide layers (Fig. 4). Rising absorption leads to a rising threshold gain and a rising carrier densities inside the quantum wells which results in more leakage. The leakage also grows with stronger carrier recombination in the waveguide layers which would lead to even less output power despite lower free-carrier density and FCA. On the other hand, higher p-doping reduces electron leakage and power saturation in our simulations.

In summary, carrier leakage and free-carrier absorption are mainly responsible for the pulse power saturation in this laser. Longitudinal spatial hole burning also causes relevant power saturation while two-photon absorption and gain compression are insignificant.

REFERENCES

- [1] I. S. Tarasov, "High-power semiconductor separate-confinement double heterostructure lasers," *Quant. Electron.*, vol. 40, no. 8, p. 661, 2010.
- [2] H. Wenzel and A. Zeghuzzi, "High-power lasers," in *Handbook of Optoelectronic Device Modeling and Simulation*. Boca Raton, FL, USA: CRC Press, ch. 27, 2017.

- [3] A. Knigge *et al.*, "Wavelength-stabilized high-pulse-power laser diodes for automotive LiDAR," *Phys. Status Solidi A*, to be published. [Online]. Available: <https://doi.org/10.1002/pssa.201700439>
- [4] J. Piprek, J. K. White, and A. J. SpringThorpe, "What limits the maximum output power of long-wavelength AlGaInAs/InP laser diodes?" *IEEE J. Quantum Electron.*, vol. 38, no. 9, pp. 1253–1259, Sep. 2002.
- [5] H. Wenzel, P. Crump, A. Pietrzak, X. Wang, G. Erbert, and G. Tränkle, "Theoretical and experimental investigations of the limits to the maximum output power of laser diodes," *New J. Phys.*, vol. 12, p. 085007, Aug. 2010.
- [6] I. S. Tarasov *et al.*, "High power CW (16 W) and pulse (145 W) laser diodes based on quantum well heterostructures," *Spectrochim. Acta A, Mol. Spectrosc.*, vol. 66, pp. 819–823, Apr. 2007.
- [7] A. Zeghuzi, M. Radziunas, H.-J. Wünsche, A. Klehr, H. Wenzel, and A. Knigge, "Influence of nonlinear effects on the characteristics of pulsed high-power broad-area distributed Bragg reflector lasers," *Opt. Quant. Electron.*, vol. 50, p. 88, Feb. 2018.
- [8] X. Wang *et al.*, "Root-cause analysis of peak power saturation in pulse-pumped 1100 nm broad area single emitter diode lasers," *IEEE J. Quantum Electron.*, vol. 46, no. 5, pp. 658–665, May 2010.
- [9] M. Dogan, C. P. Michael, Y. Zheng, L. Zhu, and J. H. Jacob, "Two photon absorption in high power broad area laser diodes," *Proc. SPIE*, vol. 8965, p. 89650P, Mar. 2014.
- [10] *PICS3D*, Crosslight Softw. Inc., Vancouver, BC, Canada, 2018.
- [11] J. Piprek and Z. M. S. Li, "On the importance of non-thermal far-field blooming in broad-area high-power laser diodes," *Appl. Phys. Lett.*, vol. 102, no. 22, p. 221110, 2013.
- [12] J. Piprek, *Semiconductor Optoelectronic Devices: Introduction to Physics and Simulation*. San Diego, CA, USA: Academic, 2003.
- [13] A. A. Said *et al.*, "Determination of bound-electronic and free-carrier nonlinearities in ZnSe, GaAs, CdTe, and ZnTe," *J. Opt. Soc. Amer. B, Opt. Phys.*, vol. 9, no. 3, pp. 405–414, 1992.
- [14] E. A. Avrutin and B. S. Ryvkin, "Theory of direct and indirect effect of two-photon absorption on nonlinear optical losses in high power semiconductor lasers," *Semicond. Sci. Technol.*, vol. 32, no. 1, p. 015004, 2017.
- [15] D. A. Veselov *et al.*, "Effect of laser cavity parameters on saturation of light—Current characteristics of high-power pulsed lasers," *Quant. Electron.*, vol. 45, no. 7, p. 597, 2015.